# **Evidence for Dynamic Primitives in a Constrained Motion Task**

James Hermus, Dagmar Sternad, and Neville Hogan

Abstract—Ten right-handed male subjects turned a crank (radius 10 cm) in two directions at three constant instructed speeds (fast, medium, very slow) with visual speed feedback. They completed 23 trials at each speed. While the hand was constrained to move in a circle, forces against the constraint were non-zero. To disentangle the influences of biomechanics and neural control we estimated a neurally-determined motion underlying the observed movements and forces. Assuming a plausible mathematical model of interactive dynamics the peripheral neuromechanics could be 'subtracted', revealing an underlying motion that reflects neural influences. We called this data-driven construct the zero-force trajectory. The observed zero-force trajectory was approximately elliptical, with systematic changes of speed with curvature, and its orientation changed with turning direction. Its major axis, estimated by the principal eigenvector of its covariance matrix, differed significantly for different directions, but not with speed. As peripheral neuromuscular compliance (i.e. low mechanical impedance) mitigates the consequences of imperfect execution, the required precision of motion commands is reduced. To produce circular hand motions, this control strategy requires an oscillatory zero-force trajectory that leads hand motion. Due to non-isotropic dynamics, that lead differs between degrees of freedom resulting in an elliptical zero-force trajectory. The ellipses' orientations differ with direction of rotation, as observed in the experimental data. As elliptical motion is generated by two orthogonal sinusoids with non-zero phase difference, these results support our hypothesis that humans simplify this constrainedmotion task by exploiting primitive dynamic actions, oscillations and impedance.

# I. INTRODUCTION

Using tools is a hallmark of human behavior, comparable to language and laughter. While some animals are capable of making and using tools, this ability is vastly more developed in humans [1]-[4]. Nonetheless, neuroscience research has primarily focused on the examination of elementary behaviors under strict experimental control (unconstrained motion). While these paradigms render manageable data for analysis and modeling, it is difficult to generalize the insights gained to understand the actions that make humans special—tool use. Physical interaction with a kinematic constraint provides an intermediate stage between unconstrained motion and physical interaction with complex dynamic objects. Moreover, kinematic constraints are ubiquitous in everyday object manipulation. Activities such as turning a steering wheel, or opening a door, are aspects of everyday life which humans perform effortlessly. This paper presents a study of unimpaired subjects physically interacting with a circular constraint—turning a crank.

While human dexterity vastly exceeds that of most modern robots, the human neuro-mechanical system is remarkably slower than its robotic counterparts [5]. We have proposed that, to achieve highly dynamic performance despite these limitations, human behavior is composed of *dynamic primitives* [6]–[9]. We conceive these to be dynamic attractors that emerge from nonlinear interactions between neural and mechanical parts of the system and require minimal intervention from higher levels of the central nervous system. In this work, we discuss two types of dynamic primitives: oscillations and mechanical impedance.

In a task that involves significant physical interaction, the mechanical impedance (interactive dynamics) of the limb relates the descending neural commands, the motion of the hand, and the force on the hand. Thus, looking at a single one of these quantities without the others would only partially explain the action.

In a previous paper, we presented the method applied in this work [10]. The approach assumes a plausible mathematical model of interactive dynamics and used it to 'subtract off' or 'peel back' peripheral biomechanics to uncover a summary of the underlying neural influences. We defined this quantity as the *zero-force trajectory*, a summary of one consequence of the underlying neural commands. Furthermore, that work showed that patterns believed to be the result of neural control re-emerge in the zero-force trajectory.

Slow neural transmission and muscle response implies that humans rely heavily on feed-forward (i.e. predictive) control; prior work shows that humans adjust their behavior to prioritize predictability [11]–[15]. The most predictable action is periodic; in theory, strictly periodic actions are infinitely predictable. Negotiating a circular constraint at constant tangential speed (equivalently: constant angular speed) requires periodic hand motion in each degree of freedom. For these reasons, we anticipate that crank-turning might preferentially be executed as an oscillatory action. Here we studied circularly constrained hand motion at constant tangential speed.

Despite the predictability of the actions required to turn a crank, imperfect execution may be anticipated due to sensor noise, motor noise, and/or inadequate prediction of inertial dynamics and neuro-muscular response. However, the

<sup>\*</sup>Research supported by NSF NRI Grant No.1637824, NIH Grant No. R01-HD087089, and the Eric P. and Evelyn E. Newman Fund.

J. Hermus is with the Department of Mechanical Engineering, Massachusetts Institute of Technology, Cambridge, MA 02139 USA (corresponding author to provide phone: 608-444-2779; (e-mail: jhermus@mit.edu).

D. Sternad is with the Departments of Biology, Electrical & Computer Engineering, and Physics, Northeastern University, Boston, MA 02115 USA

N. Hogan is with the Departments of Brain and Cognitive Sciences and Mechanical Engineering, Massachusetts Institute of Technology, Cambridge, MA 02139 USA

# CONFIDENTIAL. Limited circulation. For review only.

consequences of these imperfections should be independent of turning direction (clockwise vs. counter-clockwise). They should also decline (precipitously) with decreasing speed: all inertial forces decline as the square of speed; velocity-dependent muscle dynamics decline in proportion to speed; motor noise declines in proportion to speed; and slower speed allows ample time for feedback corrections. For this reason, we included extremely slow motions performed in both directions (CW and CCW) in our experiments.

A different source of imperfection may arise from the organization of the neural control system. In this constrained-motion task we hypothesize that humans use dynamic primitives, oscillations and impedance. This leads to a testable prediction: The underlying neural commands will exhibit differences between directions. Constant-speed circular hand motion requires sinusoidal motion in orthogonal directions with a phase offset of  $\pm 90^{\circ}$  (depending on direction CW vs. CCW). However, the motion of the hand would lag the neurally-defined oscillations to an extent determined by the slow response of the bio-mechanical periphery. This lag is likely to differ in orthogonal directions, resulting in different performance between the CW and CCW directions.

The observed zero-force trajectory was approximately elliptical. The principal eigenvector of its covariance matrix served to estimate the orientation of the ellipse major axis. As predicted, turning direction had a significant effect on the ellipse orientation, consistent with the hypothesis of dynamic primitives.

## I. METHODS

## A. Participants

Ten healthy male college-age students were recruited for the study. All participants were right-handed, and none reported any biomechanical injury to their arm nor any neurological problems. Prior to participating in the study, they were informed about the experimental procedure and signed the informed consent document approved by MIT's Institutional Review Board.

# B. Experimental Apparatus and Procedure

The crank used in this experiment is shown in Figure 1. The crank arm was mounted on a high precision incremental optical encoder/interpolator set (Gurley Precision Instruments encoder #8335-11250-CBQA, interpolator #HR2-80 QA-BRD) with a resolution of 0.0004 degrees per count. A six-axis force transducer (ATI Model 15/50) was attached to the end of the crank, with a handle mounted on it. A spool managed the force transducer cable.

During the experiment, the subject's arm was occluded from view by a wooden structure, which did not limit the range of motion. The upper arm was suspended by a canvas sling connected to the ceiling using a steel cable; upper and lower arm were in the plane of the crank. The subject sat in a chair with a rigid back, while the shoulder was constrained by a harness attached to the back of the chair. The subject was positioned such that the crank, with radius 10.29 cm, was well within the workspace of the arm.

Data acquisition was controlled by a computer running the QNX real-time operating system on an Intel Pentium 100 processor. The encoder, sampling at 200 Hz, was connected to a set of counters and to the computer via digital I/O. The ATI force transducer's signal, sampled at 100 Hz, was processed by its embedded controller and input to the computer through the digital I/O. The visual display, also generated by the computer, was on a 17-inch monitor (311 x 238 mm, resolution 1280 x 1024, 76 Hz) which was mounted approximately 75 cm from subjects' eyes. The experiment was divided into two unequal sections: 2 blocks of trials at subjects' preferred or 'comfortable' speed and 6 blocks of trials at a visually-instructed speed.

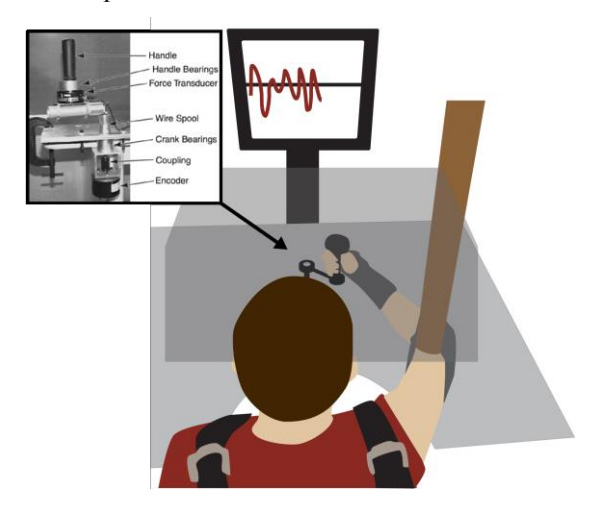


Figure 1: Experimental setup. The crank displayed in the inset was used to provide a circular constraint. Vision of the arm and crank was occluded but the subject was provided with visual speed feedback. The wrist was braced, the elbow was supported by a sling, and the shoulders were strapped to a chair.

At the start of the experiment, subjects performed 20 trials at their preferred speed, 10 trials in clockwise direction (CW) and 10 in counterclockwise direction (CCW); both conditions were blocked, in random sequence for each subject; each trial lasted 8 seconds. Subjects were not provided any visual feedback during these trials. Thereafter, subjects performed 6 blocks of 30 trials, each with visual specification of 1 of 3 target speeds (slow: 0.075, medium: 0.5, and fast: 2.0 revolutions per second), in either CW or CCW directions. The order of the speed and direction blocks was pseudorandomized across subjects. The three speeds were selected to cover a significant range: 0.075 rev/s was extremely slow (required over 13 s per revolution), 0.5 rev/s was close to subjects' preferred speed, and 2.0 rev/s was close to the fastest speed that subjects could turn the crank. Visual feedback on the monitor displayed the target speed, as well as subjects' real-time hand speed; the horizontal axis was time, and the vertical axis was speed. Subjects' speed was estimated using an online backward finite difference algorithm. Target speed was displayed as a continuous horizontal line in the middle of the screen. The relation between crank speed and screen display was re-scaled for every block; the width of the screen corresponded to the time of the trial, which was a function of the desired crank speed.

In the slow-speed conditions, each trial lasted 45 s; in the medium-speed conditions, each trial lasted 16 s; in the fast-

speed conditions, each trial lasted 4 s. This yielded 8 turns of the crank for the fast and medium conditions, but only about 3.4 turns of the crank for the slow condition. The duration of the slow-speed trials was limited to avoid subject fatigue.

#### C. Model

The arm was modeled as a two-link planar manipulator, with no gravitational effects. Inertia parameters were estimated based on the results of the cadaver studies of Dempster [16], [17]. The shoulder joint location was modeled as a fixed point, as the thorax was assumed to be stationary. The two-link manipulator dynamics coupled to the crank is detailed in Appendix. This approach is the same as used by Ohta et al. [18].

Though muscle force production is a complex function of many factors, its dominant behavior can be well described by a function of muscle length and its rate of change [19], [20]. One way to describe the dynamics of interaction uses a mechanical impedance operator  $Z\{\cdot\}$  [21]. The force F(t)time-function can be computed from the displacement timefunction  $\Delta x(t)$ ,  $F(t) = Z\{\Delta x(t)\}$ . Displacement is defined as  $\Delta x(t) = x_0(t) - x(t)$  where x(t) is the actual hand position and  $x_0(t)$  is a zero-force trajectory. Accordingly, a simplified model of muscle mechanical impedance was used—a linear spring and viscous damping element with common motion [22]. To implement this model on a two-joint arm, joint stiffness was assumed to be a 2×2 symmetric matrix, independent of configuration. Joint damping, also a 2×2 symmetric matrix, was proportional to joint stiffness. This is similar to the muscle model previously used by Flash [23] but in this case we used a damping term which was defined relative to the zero-force trajectory.

The joint torque was defined by,

$$\tau = K(q_0 - q) + B(\dot{q}_0 - \dot{q}) \tag{1}$$

The stiffness in units of N-m/rad was defined as

$$K = G \begin{bmatrix} K_{11} & K_{12} \\ K_{21} & K_{22} \end{bmatrix} = G \begin{bmatrix} 29.5 & 14.3 \\ 14.3 & 39.3 \end{bmatrix}$$
 (2)

The viscous damping in units of N-m-s/rad was defined as

$$\mathbf{B} = \begin{bmatrix} B_{11} & B_{12} \\ B_{21} & B_{22} \end{bmatrix}. \tag{3}$$

The  $K_{11}$  and  $B_{11}$  terms are the net shoulder joint stiffness and damping, the  $K_{12}$ ,  $B_{12}$ ,  $K_{21}$ , and  $B_{21}$  are the two-joint parameters, and the  $K_{22}$  and  $B_{22}$  terms describe the elbow parameters. The term G is a dimensionless scalar. The values for joint stiffness and damping were consistent with those of Flash [23], such that  $\mathbf{B} = \beta \mathbf{K}$ . The  $\beta$  term has units of time, consistent with a first-order model of muscle impedance. A gain of G = 2.0 was used in the slow and medium cases, and a gain of G = 3.0 was used in the fast case. Damping was derived from stiffness by multiplication by a constant factor,  $\beta$ , which was 0.05 s for the slow and medium cases, and 0.1 s for the fast cases.

Substituting Equation 1, into Equation 9, 10, and 11 (see Appendix), the equation can be manipulated to solve for  $\dot{q}_0$ .

$$\dot{q}_{0} = B^{-1} [MJ^{-1} [\{JM^{-1}J^{T} + r^{2}I^{-1}ee^{T}\}F 
- \dot{J}\dot{q} - r\dot{\theta} (\dot{\theta}n + b_{c}I^{-1}e)] + h - K(q_{0} 
- q)] + \dot{q}$$
(4)

Numerically integrating this first order differential equation, (Equation 4) computes the zero-force trajectory corresponding to a prescribed position, velocity, acceleration, and force.

The velocity and force signals were filtered with a second-order Butterworth filter using a cutoff frequency of 10 Hz, except in the slow tangential force condition. The tangential force in the slow condition was small in magnitude. At slow speeds, a large number of samples with a magnitude close to the resolution of the sensor were observed. This resulted in artifactual step changes in the force measurements. To eliminate this artifact, the tangential force in the slow condition was filtered with a cutoff frequency of 0.5 Hz, far faster than the turning frequency of the slow task (0.075 rev/sec).

#### D. Covariance Ellipse Orientation

To test whether the zero-force trajectory consistently changed orientation as a function of speed and direction, the zero-force trajectory covariance was computed,

$$cov(x_0, y_0) = \frac{1}{N} \sum_{i=1}^{N} (x_{0,i} - \mu_{x,0})(y_{0,i} - \mu_{y,0})$$
 (5)

where  $x_0$  and  $y_0$  are the Cartesian zero-force trajectory points,  $\mu_{x_0}$  and  $\mu_{y_0}$  are the mean Cartesian zero-force trajectory points, and N is the number of samples. The eigenvectors of this covariance matrix were computed to determine the major and minor axes of the covariance ellipse. The covariance ellipse angle was defined relative to the 3 o'clock position on the crank, consistent with the definition of crank angle. The first trial for each condition was excluded. In all subsequent trials, the first 1.5 s were discarded to remove any transient effects induced by the initial condition specified for numerical integration. Only complete revolutions were included. The dependent measure submitted to statistical analysis was the zero-force trajectory covariance ellipse angle. To statistically evaluate the influence of speed and direction, a linear mixed model was employed; it was then tested using analysis of variance (ANOVA). The linear model which represents the observed dependent measure  $Y_{i,i,k}$  was expressed as

$$Y_{i,j,k}$$

$$= \mu_T + \alpha_j + \beta_k + \gamma_l + (\alpha\beta)_{j,k} + (\alpha\gamma)_{j,l}$$

$$+ (\beta\gamma)_{k,l} + (\alpha\beta\gamma)_{j,k,l} + E_{i,(j,k,l)}$$
(6)

where the grand mean is  $\mu_T$ , the fixed effect of speed is  $\alpha_j$ , where j is an index from 1 to 3. The fixed effect of direction is  $\beta_k$ , where k is an index from 1 to 2. The random effect of subject is  $\gamma_l$ , where l is an index from 1 to 10. The stochastic sampling effect is  $E_{i,j,k}$ , where i is an index from 1 to 22, representing the multiple trials.

#### II. RESULTS

In this experiment subjects turned the planar crank at different speeds either in the CW or in the CCW direction. We hypothesized that this task was executed via dynamic primitives, leading to a testable prediction. We predicted that the underlying neural commands would be oscillatory, and exhibit differences between directions due to the phase lag introduced by peripheral neuro-mechanical dynamics. The zero-force trajectory is one consequence of the underlying neural commands; thus, it too should exhibit differences as a function of turning direction.

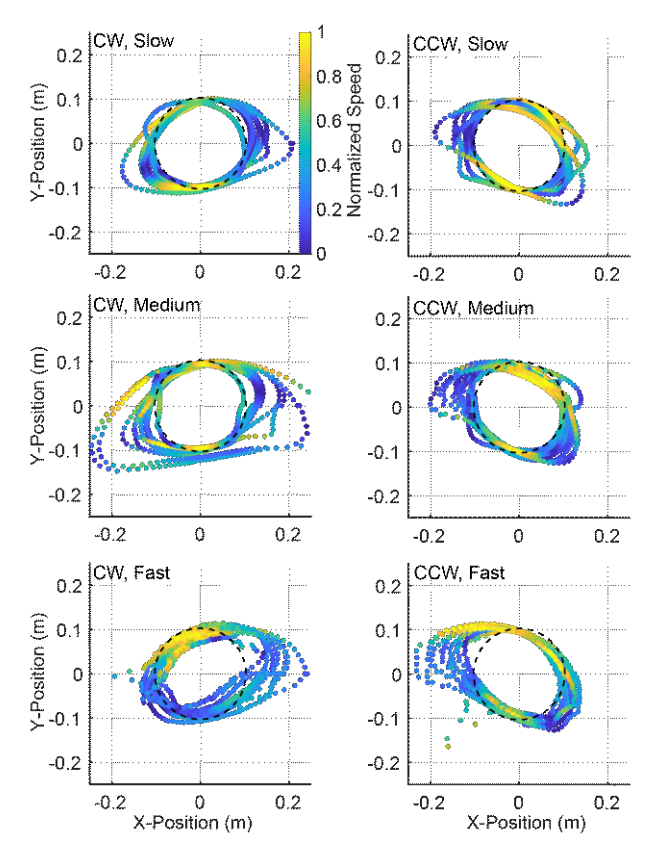


Figure 2: Average zero-force trajectories for all 10 subjects for each speed condition (left) clockwise and (right) counter-clockwise direction trials. The path defined by the constraint is shown by the black dashed circle. The zero-force trajectories are shown with colored lines indicating speed along the zero-force path normalized by its range. Note that the zero-force trajectory is roughly elliptical and that orientation differs with respect to direction.

# A. Covariance Ellipse Orientation

Figure 2 displays the average zero-force trajectories from the 10 subjects in each direction and speed condition. The shapes are approximately elliptical and show consistent speed fluctuations along the ellipse. Previous work showed that speed minima coincide with curvature maxima [10]. In addition, the elliptic shapes clearly show a difference in orientation between the two directions. To quantitatively test whether the orientation differed with respect to speed or direction the major axis angle of the covariance ellipse was computed (Figure 3). The mean major axis angle in the

clockwise conditions were (slow)  $31.78 \pm 24.22^{\circ}$ , (medium)  $30.29 \pm 16.70^{\circ}$ , and (fast)  $27.88 \pm 10.26^{\circ}$ . The mean major axis angle in the counter clockwise conditions were (slow)  $135.43 \pm 16.58^{\circ}$ , (medium)  $131.65 \pm 20.19^{\circ}$ , and (fast)  $148.94 \pm 7.55^{\circ}$ . A significant main effect of direction was detected ( $F_{1.0,9.0} = 329.021$ , p << 0.001). Thus, the zero-force trajectory was significantly different between the CW and CCW turning direction.

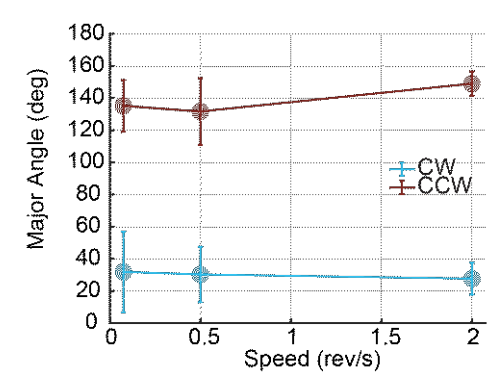


Figure 3: To quantify the zero-force trajectory orientation the covariance ellipse was computed. The plot displays the mean angle of the covariance ellipse major axis as a function of turning speed. Error bars indicate the SD between subjects.

#### III. DISCUSSION

This study examined kinematically constrained motion as an intermediate step to bridge the gap between (widelystudied) unconstrained motions and (sparsely-studied) physical interaction with objects with complex dynamics. We investigated the detailed patterns of motion and force that human subjects exhibited when performing a simple constrained-motion task, turning a circular crank. Performing this task using oscillatory dynamic primitives would require two out-of-phase sinusoids. To move in a circle, the oscillations must be  $\pm 90^{\circ}$  out of phase. Rather than attempt to execute a perfect circle, low mechanical impedance, another dynamic primitive, would obviate the need for precise motion control. However, the resulting peripheral neuro-mechanical dynamics would contribute a different phase lag in orthogonal directions. We therefore expected differences when subjects turned in opposite directions, and that was observed.

We assumed a simplified model of neuro-muscular mechanical impedance and used it to 'peel back' peripheral neuro-mechanics, and 'reveal' a consequence of underlying neural commands, expressed in terms of motion—the zero-force trajectory. The zero-force trajectory is mathematically similar to the 'virtual trajectory' of the equilibrium point hypothesis [24]–[26]. However, unlike the virtual trajectory, we are agnostic about whether the CNS encodes this quantity; many alternatives might yield similar results. Instead, the zero-force trajectory is a construct based on the measured force and motion, in combination with a reasonable, albeit simplified, model of peripheral neuro-mechanics.

The zero-force trajectory was roughly elliptical. We determined the orientation of its major axis via the principal eigenvector of the covariance matrix. The ellipse orientation was statistically independent of speed indicating that at least

some aspects of neural control of this task were the same at all speeds. Remarkably, we found that direction (CW vs. CCW) had a substantial and significant effect. This direction dependence was consistent with a neurally-defined motion command (the zero-force trajectory) composed of two sinusoids with a 90 deg phase difference.

A model that accounts for the anisotropy of skeletal inertia and neuro-muscular impedance was sufficient to explain these results. Consider the simple system where the zero-force trajectory in two orthogonal directions,  $x_0$  and  $y_0$ , is constructed from out two sinusoids with the same frequency,  $\Omega$ , same magnitude, and a phase difference,  $\phi$ .

$$\begin{cases} x_0 = \sin(\Omega t) \\ y_0 = \sin(\Omega t + \phi) \end{cases}$$
 (7)

Given such a system, a perfect circle can be drawn in the CW or CCW direction with a phase difference of  $\pm 90^{\circ}$ . However, we know that peripheral neuro-mechanical dynamics contribute a different phase lag in different directions. The work-space apparent mass of a two-link manipulator is not uniform; the mass matrix eigenvalues are not equal. This direction-dependent variation of apparent mass is one cause of the different phase lags in different directions. The additional phase lag contributed by peripheral neuro-mechanical dynamics results in zero-force trajectories with an elliptical shape that is oriented differently for CW and CCW motion. In fact, this directional effect is consistent with the change in orientation of the zero-force trajectory that we observed in our experiments.

# IV. CONCLUSION

Despite its apparent simplicity, this constrained-motion task evoked a rich set of behaviors. We observed directional differences in the zero-force trajectory orientation, consistent with task execution generated by dynamic primitives. Our observations indicate that subjects took advantage of interactive dynamics (hand mechanical impedance) to manage the control of contact and avoid the need for precise force control. The underlying motion that generated force via mechanical impedance was competently described by two oscillatory dynamic primitives, phase-shifted sinusoids. These results provide further evidence that humans manage complex physical interaction tasks by taking advantage of dynamic primitives, in this case oscillations and impedance.

## V. APPENDIX

The upper arm, forearm, hand, and forearm plus hand were denoted by 1, f, h, and 2 respectively. Each of the body segments was described by the following parameters: length, l, mass, m, inertia, l, radius of gyration,  $k_a$ , and center of mass, c. The length  $l_f$  was the distance from the elbow to the center of the fist; the length  $c_h$  was the distance from the center of the wrist to the center of the hand. Link 2 was considered a combination of the forearm and hand. The hand was assumed to be a point mass at the end of the forearm.

The model of the arm and crank system was constructed in the same manner as performed by Ohta et al. [18]. Figure 4 displays the variables and notation used in the development of the model. The system has one degree of freedom; therefore, there is always a kinematic relationship which can be used to transform from Cartesian position,  $\mathbf{x} = [x, y]^T$ , to joint position,  $\mathbf{q} = [q_1, q_2]^T$ , and to crank position,  $\theta$ , where the center of the crank is defined as  $\mathbf{x}_c = [x_c, y_c]$ .

$$x = \begin{bmatrix} l_1 C_1 + l_2 C_{12} \\ l_1 S_1 + l_2 S_{12} \end{bmatrix} = \begin{bmatrix} r \cos \theta \\ r \sin \theta \end{bmatrix} + x_c$$
 (8)

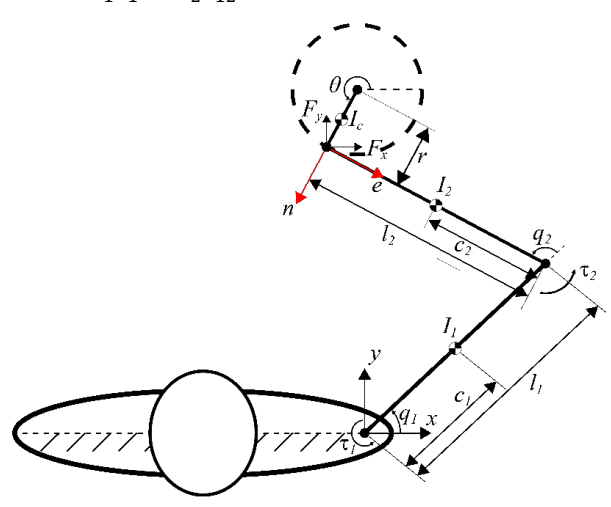


Figure 4: Model of crank rotation task which displays the sign convention and notation used in the computations.

The notation  $S_1$ ,  $C_1$  denote  $\sin(q_1)$ ,  $\cos(q_1)$  and  $S_{12}$ ,  $C_{12}$  denote  $\sin(q_1+q_2)$ ,  $\cos(q_1+q_2)$ . The radius of the crank is r, the damping of the crank is  $b_c$ , and the inertia is I. The upper arm denoted 1, and the forearm denoted 2 are described by length  $l_1$ ,  $l_2$ , mass  $m_1$ ,  $m_2$ , inertia about the z axis  $I_1$ ,  $I_2$ , and center of mass distance from the joint axis  $c_1$ ,  $c_2$ . The force on the handle is  $\mathbf{F} = \begin{bmatrix} F_x, F_y \end{bmatrix}^T$ , with the normal unit vector,  $\mathbf{n}$  and tangential unit vector,  $\mathbf{e}$ . The joint torque is denoted  $\mathbf{\tau} = \begin{bmatrix} \tau_1, \tau_2 \end{bmatrix}^T$ .

From the sum of moments acting on the crank,

$$I\ddot{\theta} + b_c \dot{\theta} = r \mathbf{e}^T \mathbf{F} \tag{9}$$

summation of moments about the shoulder,

$$\mathbf{M}\ddot{\mathbf{q}} + \mathbf{h} = \mathbf{\tau} - \mathbf{J}^T \mathbf{F} \tag{10}$$

and the kinematic relationship that equates the acceleration at the handle to the acceleration at the hand.

$$\ddot{\mathbf{x}} = \mathbf{J}\ddot{\mathbf{q}} + \dot{\mathbf{J}}\dot{\mathbf{q}} = r(\ddot{\theta}\mathbf{e} - \dot{\theta}^2\mathbf{n}) \tag{11}$$

and the joint torque was defined by,

$$\tau = K(q_0 - q) + B(\dot{q}_0 - \dot{q}) \tag{12}$$

a model of the system can be constructed. Substituting Equation 1, into Equation 9, 10, and 11 the equation can be manipulated to solve for  $\dot{q}_0$ .

$$\dot{\boldsymbol{q}}_{0}$$

$$= \boldsymbol{B}^{-1} [\boldsymbol{M} \boldsymbol{J}^{-1} [\{\boldsymbol{J} \boldsymbol{M}^{-1} \boldsymbol{J}^{T} + r^{2} \boldsymbol{I}^{-1} \boldsymbol{e} \boldsymbol{e}^{T}\} \boldsymbol{F} - \dot{\boldsymbol{J}} \dot{\boldsymbol{q}}$$

$$- r \dot{\boldsymbol{\theta}} (\dot{\boldsymbol{\theta}} \boldsymbol{n} + b_{c} \boldsymbol{I}^{-1} \boldsymbol{e})] + \boldsymbol{h} - \boldsymbol{K} (\boldsymbol{q}_{0} - \boldsymbol{q})] + \dot{\boldsymbol{q}}$$
(13)

# CONFIDENTIAL. Limited circulation. For review only.

Parameters comprising these equations include the mass matrix, the centrifugal and Coriolis forces, and the Jacobian relating unconstrained differential arm motions to hand motions.

#### ACKNOWLEDGMENT

We would like to thank Joseph Doeringer for data collection.

#### REFERENCES

- [1] G. R. Hunt, "Manufacture and use of hook-tools by new caledonian crows," *Nature*, vol. 379, no. 6562, pp. 249–251, Jan. 1996.
- [2] B. Kenward, A. A. S. Weir, C. Rutz, and A. Kacelnik, "Behavioural ecology: Tool manufacture by naive juvenile crows," *Nature*, vol. 433, no. 7022, pp. 121–121, Jan. 2005.
- [3] C. Boesch and H. Boesch, "Tool use and tool making in wild chimpanzees.," *Folia Primatol. (Basel).*, vol. 54, no. 1–2, pp. 86–99, 1990.
- [4] S. H. Johnson-Frey, "The neural bases of complex tool use in humans," *Trends Cogn. Sci.*, vol. 8, no. 2, pp. 71–78, Feb. 2004.
- [5] E. Kandel, J. Schwartz, T. Jessell, S. Siegelbaum, and A. J. Heudspeth, *Principles of Neural Science, Fifth Edition*, Fifth Edit. McGraw-Hill Education, 2013.
- [6] S.-W. Park, H. Marino, S. K. Charles, D. Sternad, and N. Hogan, "Moving slowly is hard for humans: limitations of dynamic primitives," *J. Neurophysiol.*, vol. 118, no. 1, pp. 69–83, 2017.
- [7] N. Hogan, "Physical interaction via dynamic primitives," in *Geometric and Numerical Foundations of Movements*, J.-P. Laumond, N. Mansard, and J.-B. Lasserre, Eds. Cham: Springer International Publishing, 2017, pp. 269–299.
- [8] N. Hogan and D. Sternad, "On rhythmic and discrete movements: reflections, definitions and implications for motor control," *Exp. Brain Res.*, vol. 181, no. 1, pp. 13–30, 2007.
- [9] N. Hogan and D. Sternad, "Dynamic primitives of motor behavior," *Biol. Cybern.*, vol. 106, no. 11–12, pp. 727–739, Dec. 2012.
- [10] J. Hermus, J. Doeringer, D. Sternad, and N. Hogan, "Separating Neural Influences from Peripheral Mechanics: The Speed-Curvature Relation in Mechanically-Constrained Actions," J. Neurophysiol., 2020.
- [11] P. Maurice, N. Hogan, and D. Sternad, "Predictability, force, and (anti)resonance in complex object control," *J. Neurophysiol.*, vol. 120, no. 2, pp. 765–780, Aug. 2018.
- [12] D. Sternad, "Human control of interactions with

- objects variability, stability and predictability," Springer, Cham, 2017, pp. 301–335.
- [13] B. Nasseroleslami, C. J. Hasson, and D. Sternad, "Rhythmic manipulation of objects with complex dynamics: predictability over chaos," *PLOS Comput. Biol.*, vol. 10, no. 10, pp. 1–19, Mar. 2014.
- [14] S. Bazzi, J. Ebert, N. Hogan, and D. Sternad, "Stability and predictability in human control of complex objects," *Chaos An Interdiscip. J. Nonlinear Sci.*, vol. 28, no. 10, p. 103103, Oct. 2018.
- [15] S. Bazzi and D. Sternad, "Human Manipulation of Dynamically Complex Objects through Control Control Contraction Metrics," *IEEE Robot. Autom. Lett.*, 2020.
- [16] D. I. Miller and R. C. Nelson, *Biomechanics of Sport:* a research aproach. Philadelphia: Lee and Febiger, 1973.
- [17] S. Plagenhoef, *Patterns of Human Motion: A Cinematographic Analysis*. Englewood Cliffs, NY: Prentice-Hall, 1971.
- [18] K. Ohta, M. M. Svinin, Z. Luo, S. Hosoe, and R. Laboissière, "Optimal trajectory formation of constrained human arm reaching movements," *Biol. Cybern.*, vol. 91, no. 1, pp. 23–36, 2004.
- [19] G. C. Joyce, P. M. H. Rack, and D. R. Westbury, "The mechanical properties of cat soleus muscle during controlled lengthening and shortening movements," *J. Physiol.*, vol. 204, no. 2, pp. 461–474, Oct. 1969.
- [20] P. M. H. Rack and D. R. Westbury, "The effects of length and stimulus rate on tension in the isometric cat soleus muscle," *J. Physiol.*, vol. 204, no. 2, pp. 443–460, Oct. 1969.
- [21] N. Hogan, "Impedance Control: An Approach to Manipulation: Part II—Implementation," *J. Dyn. Syst. Meas. Control*, vol. 107, no. 1, pp. 8–16, Mar. 1985.
- [22] N. Hogan, "An organizing principle for a class of voluntary movements," *J. Neurosci.*, vol. 4, no. 11, pp. 2745–2754, 1984.
- [23] T. Flash, "The control of hand equilibrium trajectories in multi-joint arm movements," *Biol. Cybern.*, vol. 57, no. 4, pp. 257–274, 1987.
- [24] E. Bizzi, N. Accornero, W. Chapple, and N. Hogan, "Arm trajectory formation in monkeys," *Exp. Brain Res.*, vol. 46, no. 1, pp. 139–143, Apr. 1982.
- [25] A. G. Feldman, "Once more on the equilibrium-point hypothesis (lambda model) for motor control.," *J. Mot. Behav.*, vol. 18, no. 1, pp. 17–54, Mar. 1986.
- [26] A. G. Feldman, "Functional tuning of the nervous system during control of movement or maintenance of a steady posture. II. Controllable paramaters of the muscles.," *Biophysics (Oxf).*, vol. 11, pp. 565–578, 1966.